ACS Catalysis

pubs.acs.org/acscatalysis Research Article

Electrocatalytic Formate Oxidation by Cobalt–Phosphine Complexes

Sriram Katipamula, Andrew W. Cook, Isabella Niedzwiecki, Chathumini Nadeesha, Ashish Parihar, Thomas J. Emge, and Kate M. Waldie*

Cite This: ACS Catal. 2025, 15, 1771–1781 Read Online

ACCESS | Metrics & More | Article Recommendations | Supporting Information

ABSTRACT: We report a family of cobalt complexes based on bidentate phosphine ligands with two, one, or zero pendent amine groups in the ligand backbone. The pendent amine complexes are active electrocatalysts for the formate oxidation reaction, generating CO_2 with near-quantitative faradaic efficiency at moderate overpotentials (0.45−0.57 V in acetonitrile). Thermodynamic measurements reveal that these complexes are energetically primed for formate oxidation via hydride transfer to the cobalt center, followed by deprotonation of the resulting cobalt-hydride by formate acting as a base. The complex featuring a single pendent amine arm is the fastest electrocatalyst in this series, with an observed rate constant for formate oxidation of 135 ± 8 h^{-1} at 25 °C, surpassing the activity of the bis-pendent amine analogue. Electrocatalytic turnover is not observed for the complex with no pendent amine groups: decomposition of the complex is evident in the presence of high formate concentrations. Thus, the application of thermodynamic considerations to electrocatalyst design is demonstrated as a successful strategy, while also highlighting the delicate balance of ligand properties necessary for achieving productive turnover.

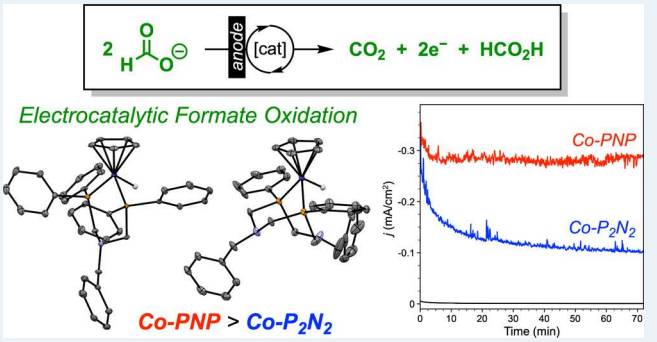

KEYWORDS: *cobalt complexes, formate oxidation, electrocatalysis, hydricity, pendent amines*

INTRODUCTION

The exploration of chemical fuels as energy carriers to bridge the gap between intermittent renewable electricity availability and global energy demand continues to be a major research theme. While renewably sourced H_2 has drawn considerable interest as an energy carrier to mitigate our reliance on fossil resources for energy production,[1−4] the challenges associated with the safe storage and transportation of H_2 fuel remain.[5] Formic acid represents an appealing alternative to H_2, offering distinct advantages in terms of safety, storage, and handling thanks to its liquid state, chemical stability, low ignition point, and low toxicity.[6,7] Thus, continued research into electrocatalysts capable of mediating the $2e^-$,$1H^+$ oxidation of formate is crucial for deepening our understanding of the thermodynamic and kinetic factors required to selectively achieve this transformation (Figure 1a).[8]

Heterogeneous electrocatalysts for formate oxidation are largely based on noble metal systems and can suffer from catalyst poisoning due to competitive CO production.[8−13] Homogeneous electrocatalysts often operate with high selectivity due to precise active site structures and reaction mechanisms; however, to the best of our knowledge, only four families of homogeneous electrocatalysts for formate oxidation have been reported to date (Figure 1b).[14−18] Appel, Kubiak, and co-workers disclosed the first example utilizing a series of nickel P_2N_2 electrocatalysts, where P_2N_2 = 1,5-diaza-3,7-diphosphacyclooctane.[14,15] The pendent amines in the P_2N_2 ligand were critical for electrocatalytic turnover: the nickel depe analogue was not an active electrocatalyst (depe = 1,2-bis(diethylphosphino(ethane)). While the precise mechanism of formate oxidation remains in question,[15,19] direct hydride transfer from formate to the Ni^{II} center to generate a Ni^{II}-hydride intermediate may be operative. Later work by Kang and co-workers achieved bidirectional formate oxidation-CO_2 reduction using an iridium pincer electrocatalyst.[17] Yang and co-workers developed a reversible electrocatalytic system for formate-oxidation-CO_2 reduction based on a platinum diphosphine complex.[18] For the two noble metal systems, formate oxidation was proposed to occur through hydride transfer. More recently, an iron-thiolate electrocatalyst was reported to achieve rapid formate oxidation by a net hydride

Received: May 30, 2024
Revised: January 8, 2025
Accepted: January 8, 2025
Published: January 17, 2025

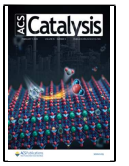

https://doi.org/10.1021/acscatal.4c03189
ACS Catal. 2025, 15, 1771−1781

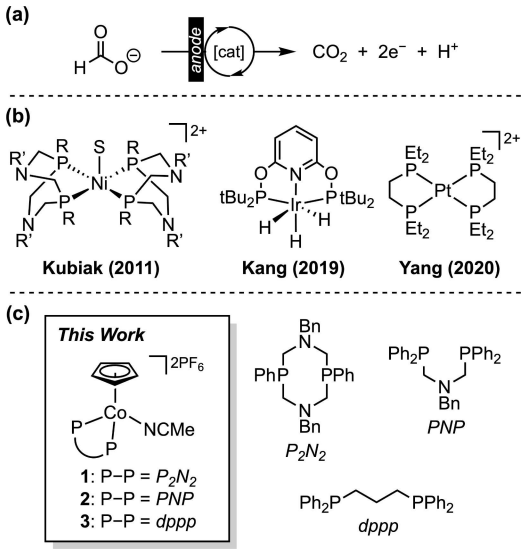

Figure 1. (a) Electrocatalytic formate oxidation. (b) Previous examples of molecular electrocatalysts for formate oxidation.[14−18,37] (c) Cobalt complexes **1**−**3** from this work.

transfer mechanism where the electrons and proton are not colocated, but significant operating potentials were required.[20]

The favorability of hydride transfer reactions can be quantified using thermodynamic hydricity.[21] The hydricity of the formate anion in acetonitrile is 44 kcal/mol.[22] To promote heterolytic cleavage of the formate C−H bond via hydride transfer to a metal center, the hydricity of the resulting metal-hydride bond must be greater than this value. We[23] and others[24,25] have previously reported $CpCo^{III}$(diphosphine)-hydride complexes (Cp = cyclopentadienyl ligand) to have hydricities near 70 kcal/mol. Thus, this architecture should be poised for energetically favorable formate oxidation. We note that select $CpCo^{II}$-hydrides have been utilized for electrocatalytic reduction reactions including H_2 evolution and CO_2 reduction to formate due to their much stronger hydride donating abilities;[25−28] however, Co^{III}-hydrides have not yet been explored within the context of electrocatalysis.

The anticipated thermodynamic driving force for hydride transfer from formate to Co^{III} centers motivated us to prepare a series of $[CpCo^{III}(P{-}P)(MeCN)]^{2+}$ complexes **1**-**3** (Figure 1c). Phosphine ligands with pendent amine groups have featured prominently in several electrocatalytic systems for facilitating intramolecular proton transfer and stabilizing transition states.[28−36] Pendent amines are central to the electrocatalytic activity of the nickel P_2N_2 systems for formate oxidation,[14] and the P_2N_2 ligand is proposed to form a hydrogen bonding network to achieve efficient CO_2 reduction at $CpCo^{II}$-hydrides.[28] Inspired by these reports, we targeted complexes containing the P_2N_2 ligand as well as the related PNP and dppp ligands, which have one and zero pendent amine groups, respectively. Herein, we report our investigations into this family of cobalt complexes and show that **1** and **2** are active electrocatalysts for the selective oxidation of formate to CO_2 at ambient conditions. The thermodynamic properties of these complexes are reported, which confirm the high hydride affinity of **1**−**3**. The electrocatalytic activity for formate oxidation is quantified by chronoamperometry and controlled-potential electrolysis, revealing **2** as the best performing electrocatalyst in this series.

RESULTS AND DISCUSSION

Synthesis and Characterization. The PNP and P_2N_2 ligands were synthesized following literature procedures.[38,39] Complexes **1**−**3** were prepared by the reaction of the desired phosphine ligand with $[CpCo(CO)I_2]$, followed by halide abstraction using $AgPF_6$ (2.2 equiv) (Scheme 1).[40] Each

Scheme 1. Synthesis of Complexes 1−9

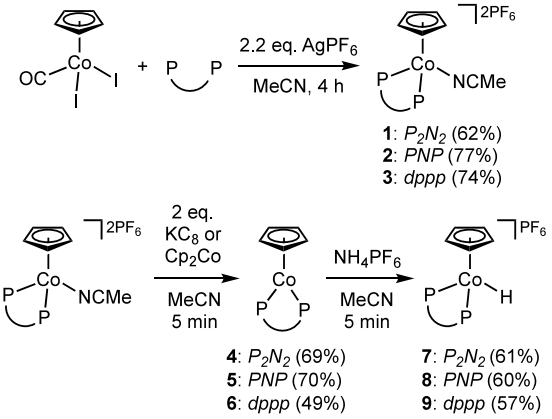

complex was isolated as a red crystalline solid in reasonable yield following recrystallization from diethyl ether/acetonitrile. These complexes are air and moisture stable in solution over several days. The ^1H NMR spectra of **1**-**3** show a sharp singlet at 5.5−5.7 ppm corresponding to the Cp ligand. The $^{31}P\{^1H\}$ NMR spectra display one singlet for the phosphine ligand near 30 ppm. These values are typical of $CpCo^{III}$-phosphine complexes and indicate that the pendent amine groups do not substantially influence the NMR characteristics of these systems.[23,28,41,42]

The synthesis of the Co^I (**4**−**6**) and Co^{III}-hydride (**7**−**9**) complexes was adapted from literature procedures for related systems (Scheme 1).[25] In brief, complexes **1**−**3** were treated with 2 equiv chemical reductant (KC_8 or cobaltocene) to obtain **4**−**6** as dark red solids, and subsequent protonation with 1 equiv NH_4PF_6 yielded Co^{III}-hydrides **7**−**9** as bright yellow crystalline powders. We note that while **7**−**9** are highly air-sensitive, they remain stable in acetonitrile under N_2 for several days. By ^1H NMR, the Cp signals of **4**−**6** are observed at 4.4−4.5 ppm, shifted upfield by more than 1 ppm compared to the respective signals in **1**−**3**. These chemical shift changes are consistent with a decrease in metal oxidation state and overall complex charge upon reduction from $[Co^{III}\text{-}MeCN]^{2+}$ to $[Co^I]^0$. This signal is shifted downfield to ca. 4.8 ppm for Co^{III}-hydride **7**−**9**, as expected for protonation of $[Co^I]^0$ to $[Co^{III}{-}H]^+$.[41,42] The diagnostic ^1H NMR hydride signal for **7**−**9** appears as a well-resolved triplet at ca. −14 ppm. As with **1**−**3**, the phosphorus ligand identity has minimal effect on the NMR spectra for this series.

Crystals suitable for X-ray crystallography were obtained via vapor diffusion of diethyl ether into acetonitrile (for **3**, **7**, and **9**) or dichloromethane (for **2**), or by slow cooling of a concentrated solution in acetonitrile (for **4** and **5**), tetrahydrofuran/diethyl ether (for **6**), or acetonitrile/diethyl ether (for **8**). The structures of the PNP complexes are highlighted in Figure 2. All other structures, along with select structural metrics, are provided in the Supporting Information. The structure of **1** was previously reported by Artero and coworkers.[28] All Co^{III} complexes adopt a three-legged piano-stool

https://doi.org/10.1021/acscatal.4c03189
ACS Catal. 2025, 15, 1771−1781

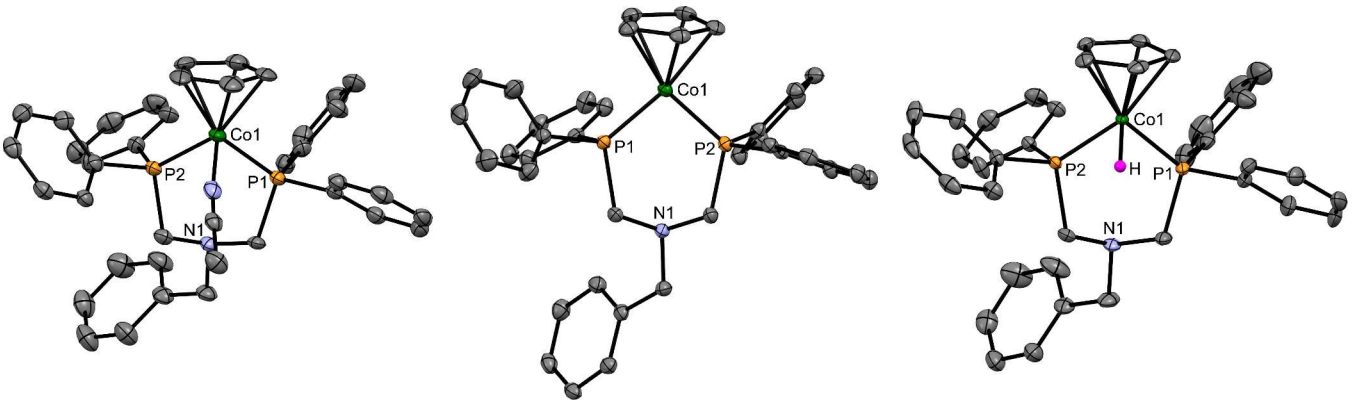

Figure 2. Structures of PNP complexes **2** (left), **5** (center), and **8** (right). Hydrogen atoms, cocrystallized solvent molecules, and PF_6^- counterions are omitted for clarity. Ellipsoids are shown at 50% probability.

geometry with the planar η^5-Cp ligand and bidentate phosphine ligand. The final coordination site is occupied by either acetonitrile (**1**–**3**) or hydride (**7**–**9**). The PNP and dppp ligands both form a six-membered metallocycle in a chair conformation with the Co^{III} center, while the P_2N_2 in **7** forms two six-membered rings analogous to **1**: one in a chair conformation, one in a boat conformation. The structures of **4**–**6** exhibit a two-legged piano-stool geometry, which is typical of half-sandwich Co^I complexes.[23] The η^5-Cp ligand and the P1–Co–P2 plane are approximately perpendicular. There is a general increase in the Co–P bond lengths within each compound class following P_2N_2 < PNP < dppp. This trend is consistent with the greater electron donating character of the P_2N_2 ligand in which each phosphine has one phenyl and two alkyl groups, as opposed to the one alkyl and two phenyl groups in the PNP and dppp ligands.

Electrochemical Studies. Cyclic voltammetry (CV) was used to probe the electrochemical behavior of **1**–**3** in 0.1 M [^{n}Bu$_4$N][PF$_6$] in acetonitrile. Each complex displays two reversible one-electron reductions (Figure 3 and Table 1), which are assigned to the Co^{III}-MeCN/Co^{II} and Co^{II}/Co^I couples, respectively.[21,23,26,28,41,42] These assignments are corroborated by the CV response in dichloromethane, where reduction of Co^{III}-MeCN is chemically irreversible (Figures S43–S45). In all cases, the peak currents vary linearly with the square root of the scan rate ($v^{1/2}$), indicating diffusion-controlled electron transfer (Figures S37–S42). Complexes **2** and **3** exhibit very similar potentials for both redox processes (within 50 mV), while the reduction potentials for **1** are ca. 200 mV more negative. As noted above, this trend is consistent with the greater electron donating character of the P_2N_2 ligand.

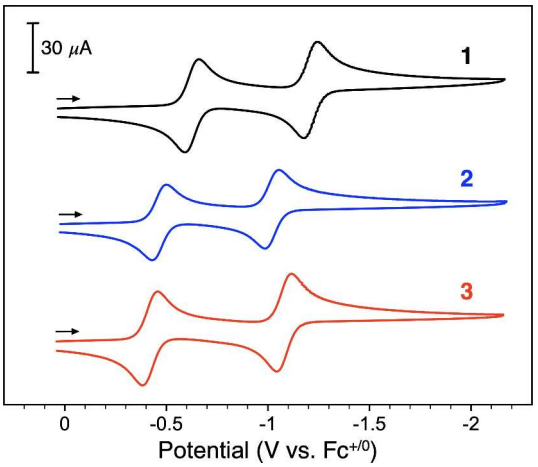

Figure 3. CVs of **1** (black), **2** (blue), and **3** (red) in acetonitrile. Scan rate = 100 mV/s.

Table 1. CV Data for Complexes 1–3[a]

complex	$E_{1/2}$ (V)[c]	ΔE_p (mV)[d]	i_c/i_a[e]	$E_{1/2}$ (V)[c]	ΔE_p (mV)[d]	i_c/i_a[e]
1	−0.64	84	1.03	−1.21	91	1.01
2	−0.47	68	0.98	−1.02	63	1.01
3	−0.42	72	1.05	−1.07	66	1.06
1[b]	−0.95	106	1.08	−1.21	72	1.01
2[b]	−0.83	76	1.05	−1.02	68	1.00
3[b]	−0.75	70	1.02	−1.08	67	1.01

[a]1 mM [Co] in 0.1 M [^{n}Bu$_4$N][PF$_6$] in acetonitrile, glassy carbon working electrode, Pt wire counter electrode, Ag/AgNO$_3$ reference electrode. 100 mV/s. [b]With 10 mM [^{n}Bu$_4$N][HCO$_2$]·HCO$_2$H. [c]$E_{1/2}$ = (E_{pa} + E_{pc})/2, where E_{pa} and E_{pc} are anodic and cathodic peak potentials, respectively. Potentials in V vs $Fc^{+/0}$. [d]$\Delta E_p = E_{pa} - E_{pc}$. [e]$i_c$ = cathodic peak current; i_a = anodic peak current.

Thermodynamic Properties. Given the relevance of thermodynamic hydricity (ΔG_{H-}) to formate oxidation, we sought to experimentally determine this value for Co^{III}-hydrides **7**–**9**. There are three established methods for measuring the hydricity of metal-hydride complexes: here, we use the *potential-pK_a* approach outlined in Scheme 2.[21] In this thermochemical cycle, the free energy associated with the Co^{III}-MeCN/Co^{II} and Co^{II}/Co^I redox couples and the acidity of the Co^{III}-hydride are combined with the free energy for two-

Scheme 2. Potential-pK_a Method for Determining the Hydricity of Co^{III}-Hydrides 7–9[a]

$$[L_nCo^{III}\text{–}H]^+ \rightleftharpoons [L_nCo^{I}] + H^+ \qquad 1.364\ pK_a \qquad (1)$$

$$[L_nCo^{I}] \rightleftharpoons [L_nCo^{II}]^+ + e^- \qquad 23.06\ E_1^\circ \qquad (2)$$

$$[L_nCo^{II}]^+ \overset{S}{\rightleftharpoons} [L_nCo^{III}\text{–}S]^{2+} + e^- \qquad 23.06\ E_2^\circ \qquad (3)$$

$$H^+ + 2\,e^- \rightleftharpoons H^- \qquad 79.6 \qquad (4)$$

$$[L_nCo^{III}\text{–}H]^+ \overset{S}{\rightleftharpoons} [L_nCo^{III}\text{–}S]^{2+} + H^- \qquad \Delta G^\circ_{H-} \qquad (5)$$

$$\Delta G^\circ_{H-} = 1.364\ pK_a + 23.06\ E_1^\circ + 23.06\ E_2^\circ + 79.6 \qquad (6)$$

[a]S = acetonitrile. Reaction free energies in kcal/mol.

https://doi.org/10.1021/acscatal.4c03189
ACS Catal. 2025, 15, 1771–1781

electron reduction of a proton to obtain the thermodynamic hydricity according to eq 6.[43] As noted with other systems, this value could be considered an *effective hydricity* measurement since coordination of an acetonitrile ligand to the Co^{III} center occurs following hydride loss from the Co^{III}-hydride, and thus the free energy associated with this coordination event is implicitly included in this calculation.[44]

The relevant redox potentials for **1**−**3** were measured by CV (*vide supra*). The pK_a of Co^{III}-hydride **7**−**9** was measured by UV−vis spectrophotometric titration in acetonitrile/toluene (90:10) to solubilize both the Co^{III}-hydride and Co^{I} complexes.[41,42] Addition of an appropriate base, either triethylamine (pK_a = 18.4)[45] or DBU (1,8-diazabicyclo[5.4.0]-undec-7-ene, pK_a = 24.3),[45] to a 0.55 mM solution of Co^{III}-hydride **7**−**9** leads to formation of the conjugate base **4**−**6**, respectively (Figures S60−S62). The initial and final absorbance spectra in these titrations match the UV−vis spectra of independently prepared solutions of each Co-hydride and Co^{I} complex (Figures S48−S59). From these data, the pK_a of **8** and **9** are calculated to be identical within experimental error (pK_a = 19.8), while the pK_a of **7** is 23.1 (Table 2). These results are consistent with the greater electron donating character of the P_2N_2 ligand (*vide supra*): the dppp and PNP ligands both contain an alkyl-type backbone and two phenyl substituents on each phosphorus, resulting in comparable properties at the metal center for **8** and **9**. The presence of the pendent amine group in **8** does not significantly affect the thermodynamics of proton transfer compared to the dppp analogue.

Table 2. Summary of Electrochemical and Thermodynamic Data in Acetonitrile

ligand	$E_{1/2}[Co^{III/II}]^a$	$E_{1/2}[Co^{II/I}]^a$	pK_a of Co^{III}−H	ΔG_{H-} of Co^{III}−H[b]
P_2N_2	−0.64	−1.21	23.1 ± 0.4	68.5 ± 0.6
PNP	−0.47	−1.02	19.8 ± 0.3	72.3 ± 0.5
dppp	−0.42	−1.07	19.8 ± 0.3	72.3 ± 0.5
dppe[42]	−0.51	−0.93	18.4	71.5[24]
dcpa[23]	−0.53	−1.22	23.2	71.0

[a]Potential in V vs $Fc^{+/0}$. [b]Hydricity (ΔG_{H-}) in kcal/mol.

Using eq 6 and the experimental redox and pK_a data, we obtain the thermodynamic hydricity of each Co^{III}-hydride (Table 2). The P_2N_2 complex **7** is the strongest hydride donor in this series, with ΔG_{H-} = 68.5 kcal/mol. The PNP and dppp complexes (**8** and **9**, respectively) both have hydricity values of 72.3 kcal/mol, making these species slightly poorer hydride donors compared to **7**. Previous reports have demonstrated linear correlations between the thermodynamic hydricity and the first reduction potential of the parent complex, and between the pK_a and the second reduction of the parent complex for several nickel,[21] palladium,[46] and other[24,47] hydrides. As expected, these cobalt systems display similar linear trends, which also considers data for the dppe[24,42] and dcpa[23] analogues (dcpa = bis(dicyclophosphino)methylamine) reported elsewhere (Figures S63−S64). As with the pK_a values, the hydricity values of **7**−**9** are largely governed by the inductive properties of the phosphine substituents. We note that hydride affinity is given by the reverse reaction of hydricity (i.e., hydride affinity = $-\Delta G_{H-}$): thus, the P_2N_2 complex **1** is the weakest hydride acceptor in this series, while PNP and dppp complexes (**2** and **3**, respectively) have similar hydride affinities.

Chemical Reactivity Studies with Formate. The hydricity of formate in acetonitrile is 44 kcal/mol.[22] Given the experimentally determined hydricity values for **7**−**9** (Table 2), the hydride affinity of each Co^{III}-acetonitrile complex is such that hydride transfer from formate to the metal center is predicted to be highly thermodynamically favorable. We first sought to investigate the chemical reactivity of **1**−**3** with formate under pseudo-first order conditions. For these studies, we used an acetonitrile-soluble tetrabutylammonium formate salt, which has been shown to crystallize as the 1:1 formate:formic acid adduct $[^nBu_4N][HCO_2]\cdot HCO_2H$.[14] Thus, this salt provides a buffered formate:formic acid solution for analysis. For simplicity, we will refer to $[^nBu_4N][HCO_2]\cdot HCO_2H$ as formate in this article, unless otherwise specified.

Treatment of **1** or **2** with 15 equiv formate in CD_3CN results in the generation of the corresponding Co^{I} species **4** or **5** based on ^1H NMR (Figure S74−S75). We repeated this experiment on a larger scale in a gastight flask and sampled the reaction headspace by gas chromatography. Quantitative formation of CO_2 (relative to cobalt) is observed after 150 s, confirming stoichiometric formate oxidation (Scheme 3 and Table S11).

Scheme 3. Proposed Stepwise Reactivity of 2 with 15 equiv $[^nBu_4N][HCO_2]\cdot HCO_2H$[a]

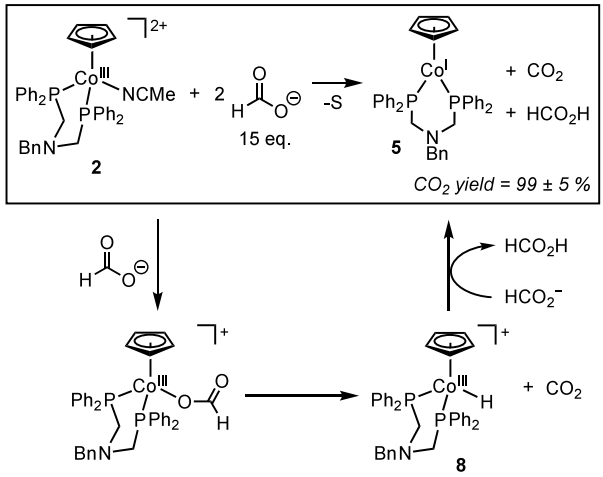

[a]S = acetonitrile.

The formation of the Co^{I} complex in these studies is consistent with initial hydride transfer from formate to generate the Co^{III}-hydride, followed by deprotonation of the Co^{III}-hydride where an additional equivalent of formate acts as a base. The estimated pK_a of formic acid in acetonitrile is 20.9,[48] which is in a similar range as the pK_a values of **4**−**6** and suggests that a reversible proton transfer equilibrium may be accessible from the reaction of the Co^{III}-hydrides and formate. Indeed, in separate experiments, we find that treatment of the Co^{III}-hydrides with 15 equiv formate results in rapid proton transfer and the formation of the Co^{I} complexes (Figures S89 and S90). The addition of 15 equiv formate to **3** also results in formate oxidation to CO_2; however, the CO_2 yield relative to cobalt is lower (63 ± 5%) and free dppp ligand is observed by $^{31}P\{^1H\}$ NMR (Figure S77), indicating that this complex undergoes partial decomposition in the presence of formate. Together, these initial experiments indicate that **1** and **2** are

https://doi.org/10.1021/acscatal.4c03189
ACS Catal. 2025, 15, 1771−1781

capable of key chemical steps for formate oxidation to CO_2 and are viable electrocatalyst candidates, while **3** shows limited stability in the presence of high formate concentrations.

We conducted further studies to investigate the reactivity of **1**−**3** with formate at lower formate concentrations in an effort to observe the putative reaction intermediates depicted in Scheme 3. Upon addition of 1 equiv formate to **1** or **2** in CD_3CN, a new species is immediately observed by ^{1}H NMR, which is assigned as the Co^{III}-formate intermediate (Figures S78 and S81). This species is also presumably formed at higher formate concentrations but is not detected by ^{1}H NMR due to its fast conversion. Resonances associated with a paramagnetic species are also observed by ^{1}H NMR, which slowly increase in concentration over time as the Co^{III}-formate signals decrease. The paramagnetic species is attributed to $[CpCo^{II}(P{-}P)]^+$, which is supported by comparison to our recently reported characterization of $[CpCo^{II}(P_2N_2)]^+$.[49] After 1 h, signals for Co^{III}-hydride **7** or **8** appear and gradually continue to increase, reaching ca. 60% and 95% conversion to the Co^{III}-hydride after 10 h, respectively (Figures S79−S80 and S82−S83).

Unlike in the presence of excess formate (15 equiv), complex **3** shows good stability at low formate concentrations, enabling comparison of the reactivity of all three complexes (i.e., **1**−**3**) in the presence of 1 equiv formate. As shown in the Supporting Information, **3** is initially converted to the corresponding Co^{III}-formate adduct, the concentration of which gradually decreases in the first 1−2 h. The formate C−H signal occurs at 8.21 ppm.[50] Paramagnetic signals assigned as $[CpCo^{II}(dppp)]^+$ increase then decay over time, based on comparison to an independently prepared sample obtained via chemical reduction of **3** with 1 equiv cobaltocene (Figure S85). After 10 h, ca. 50% conversion to the Co^{III}-hydride **9** is achieved. While small variations in the formate loading and composition of the formate buffer[51] were found to affect the rate of the overall reaction, the general reactivity trend follows as PNP > P_2N_2 > dppp.

We recently reported the similar reactivity of the related [CpCo-dcpa] complex at 65 °C in the presence of stoichiometric formate.[23] We propose the same reactivity pathway is operative with **1**−**3** at 25 °C (Scheme 4). Following the initial formation of the observed Co^{III}-formate intermediate, slow hydride transfer yields the Co^{III}-hydride, which is immediately deprotonated by formate. Under these stoichiometric conditions, the hydride transfer step is sufficiently slow, allowing the resulting Co^{I} intermediate to comproportionate with the remaining Co^{III}−X (X = MeCN or formate), which accounts for the unexpected observation of the paramagnetic Co^{II} complex. Indeed, attempts to isolate single crystals of $[CpCo(dppp)(formate)]^+$ instead yielded crystals of $[CpCo^{II}(dppp)]^+$ (Figure S9), supporting the presence of this species in this reaction mixture. In further support of this proposal, we note that the comproportionation reaction of Co^{I} with Co^{III}−X for each ligand system is very favorable, which is readily obtained from the difference in $Co^{III/II}$ and $Co^{II/I}$ redox potentials (Scheme 4 and Table S12). The rate of comproportionation was too fast to measure by UV−vis stopped-flow methods; nonetheless, this provides a lower bound for the second-order comproportionation rate constant ($k_{comp} > 10^8$ M^{-1} s^{-1}), from which the lower limit for the disproportionation rate constant can be estimated (see Supporting Information). We also observe that protonation of Co^{I} complexes **4**−**6** with formic acid (>2 equiv) is rapid, leading to *in situ* Co^{III}-hydride formation (see Supporting Information).[52] From this data, the second-order rate constant for the protonation of Co^{I} can be determined. By combining this data with the equilibrium constant for reversible proton transfer, the rate constant for the reverse reaction, deprotonation of the Co^{III}-hydride, can be estimated (Scheme 4). From this data, we find that the proton transfer equilibrium is rapid at 25 °C. The gradual conversion to the Co^{III}-hydride complex occurs as the reaction solution becomes more acidic and the irreversible loss of CO_2 via formate oxidation drives the reversible comproportionation/disproportionation and proton transfer equilibria to the final Co^{III}-hydride species. We note that Kurtz and Dempsey reported the related reactivity of the $[CpCo^{II}(dppe)]^+$ derivative, which yielded the Co^{III}-hydride and Co^{III}−OR complexes (OR = conjugate base of the Brønsted acid) upon treatment with Brønsted acids via disproportionation of the Co^{II} and subsequent protonation of the Co^{I}.[53]

Scheme 4. Proposed Reaction Scheme for the Reactivity of 1−3 at Lower Formate Concentrations; Summary of Thermodynamic and Kinetic Data for the Deprotonation ($K_{DT} = k_{DT}/k_{PT}$) and Comproportionation (K_{comp}) Equilibria[a]

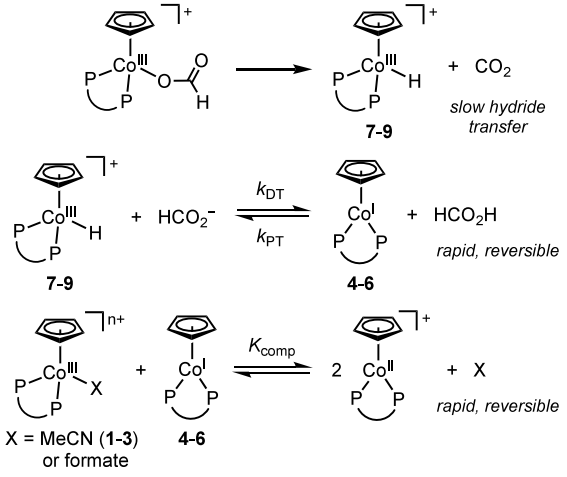

ligand	K_{DT}	k_{DT} (M^{-1} s^{-1})	k_{PT} (M^{-1} s^{-1})	K_{comp} (X = MeCN)	K_{comp} (X = formate)
P_2N_2	0.00631	3.0×10^4	4.8×10^6	4.37×10^9	2.50×10^4
PNP	12.6	2.1×10^7	1.7×10^6	2.00×10^9	1.63×10^3
dppp	12.6	3.3×10^7	2.6×10^6	9.85×10^{10}	3.81×10^5

[a]X = MeCN or formate.

The above studies indicate that the Co^{III}-hydride is the final product from this series of reactions at lower formate concentration as the solution gradually becomes more acidic and the conversion of formate to CO_2 occurs irreversibly; however, initial Co^{III}-hydride formation via hydride transfer was not directly observed. Considering hydride transfer as the rate-limiting step, rapid deprotonation of the resulting Co^{III}-hydride by the formate buffer ensures that the concentration of this species remains negligible. While the reaction is much slower under stoichiometric conditions, Co^{III}-hydride accumulation is still prevented by the subsequent fast and favorable deprotonation-comproportionation equilibria. Aiming to disfavor deprotonation of the Co^{III}-hydride, we prepared a series of formate:formic acid solutions where the acidity was incrementally increased using HBF_4. However, this approach was unsuccessful, as either the comproportionation pathway

https://doi.org/10.1021/acscatal.4c03189
ACS Catal. 2025, 15, 1771−1781

was still observed or formate oxidation was entirely hindered at higher acidity levels. We also examined formate oxidation at higher temperatures to increase the rate of hydride transfer. Complex **2** was treated with 1 equiv formate in acetonitrile/toluene (1:1) at 100 °C. After 5 min, ^{1}H NMR analysis confirmed Co^{III}-hydride **8** formation (Scheme 5). While not directly comparable to experiments performed at ambient temperature, this result suggests that formate oxidation proceeds via hydride transfer to the metal.

Scheme 5. Formation of Co^{III}-Hydride 8 at Elevated Temperatures

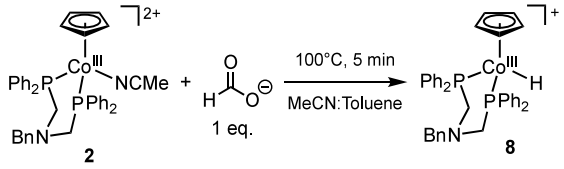

Electrocatalytic Formate Oxidation. Our chemical reactivity studies clearly indicate that **1** and **2** can mediate stoichiometric formate oxidation to generate CO_2 in quantitative yield. Thus, we also investigated their activity for the electrocatalytic oxidation of formate by electrochemical methods. Upon addition of 10 equiv formate to the CV solution of **1**−**3**, the open-circuit potential of the electrochemical cell changes dramatically (Figure 4a and S46−S47), shifting from ca. 0 V vs Fc$^{+/0}$ in the absence of formate (more positive than the Co^{III}-MeCN/Co^{II} redox couple) to ca. −1.5 V vs Fc$^{+/0}$ with formate added (more negative than the Co^{II}/Co^{I} redox couple). This behavior is indicative of a significant change in the composition of the bulk solution, and is consistent with the formation of Co^{I} according to Scheme 3. Electrochemical oxidation of the Co^{I} complex occurs as the potential is swept in the positive direction; however, the CV data does not show appreciable current enhancement, indicating that electrocatalytic turnover is not observable on this time scale.

The CV studies of **1**−**3** in the presence of formate also reveal a significant shift (ca. 300 mV) in the Co$^{III/II}$ redox couples to more negative potentials (Figure 4a and S46−S47). Previous work by Dempsey and co-workers showed that [CpCo(P−P)(MeCN)]$^{2+}$ complexes undergo one-electron reduction by an E_rC_r mechanism where reversible dissociation of the acetonitrile ligand occurs at the Co^{II} state.[41,42] Given this precedent, an E_rC_r mechanism involving formate is reasonable, where one-electron reduction of the Co^{III}-formate complex is followed by the reversible dissociation of formate from the Co^{II} state. Since formate is an anionic ligand, the Co^{III}-formate/Co^{II} couple occurs at a more negative potential compared to that of the Co^{III}-acetonitrile complex. The Co$^{II/I}$ redox couple is unaffected by the presence of formate in solution (Table 1).

Since electrocatalytic currents were not observed by CV, we turned to chronoamperometry (CA) to further probe the reactivity of **1** and **2** with formate. CA methods can be utilized to extract an observed rate constant (k_{obs}) for electrocatalytic reactions, and this approach can be especially useful for reactions where $k_{obs} < 1\ s^{-1}$.[52,54] For our CA studies, we started with Co^{I} complex **4** or **5** (0.5 mM) in 0.1 [^{n}Bu$_4$N][PF$_6$] in acetonitrile such that an oxidative potential step could be applied to the system. Formate (50 equiv) was added to the solution and the CA experiment was repeated. In each case, the applied potential was held 200 mV more positive than the appropriate Co$^{III/II}$ redox potential: Co^{III}-MeCN/Co^{II} or Co^{III}-formate/Co^{II} for 0 or 50 equiv formate, respectively. As shown in Figure 4b, current enhancement is achieved with **5** in the presence of formate, indicating electrocatalysis (Figure 4b). The ratio of these two CA traces was fit to the equation describing an *EC′* mechanism (see Supporting Information), from which k_{obs} is estimated to be 135 ± 8 h^{-1}. With complex **4**, the CA traces are identical within experimental error (Figure S65), indicating that any electrocatalysis is too slow to quantify by this technique; we estimate the upper limit for electrocatalytic formate oxidation to be 4 h^{-1}.

To confirm electrocatalytic formate oxidation with **1** and **2**, we examined their electrocatalytic behavior by controlled-potential electrolysis (CPE). In these studies, the working electrode potential was held ca. 150 mV more positive than the Co^{III}-formate/Co^{II} couple to ensure rapid electron transfer.

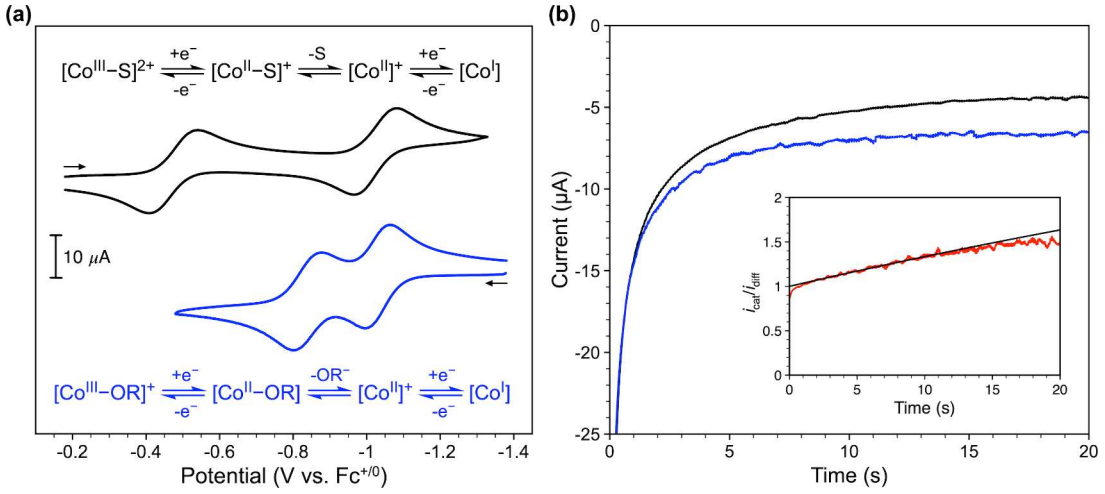

Figure 4. (a) Cyclic voltammograms and proposed reactivity pathways for **2** (0.5 mM, black) and **2** with 10 equiv [^{n}Bu$_4$N][HCO$_2$]·HCO$_2$H (blue) in acetonitrile. S = acetonitrile. OR$^-$ = formate. Scan rate = 100 mV/s. (b) Chronoamperometry of **5** (0.5 mM, black) and **5** with 50 equiv [^{n}Bu$_4$N][HCO$_2$]·HCO$_2$H (blue) in acetonitrile at η = 200 mV (E_{app} = −0.27 and −0.63 V vs Fc$^{+/0}$, respectively). Inset: Current ratio of the chronoamperometry traces (red) and fit between 5 and 10 s (black).

https://doi.org/10.1021/acscatal.4c03189
ACS Catal. 2025, 15, 1771−1781

Using **1** or **2** in the presence of 50 equiv formate, a stable current was obtained, with **2** consistently achieving higher current densities (Figure 5). After 95 min, analysis of the

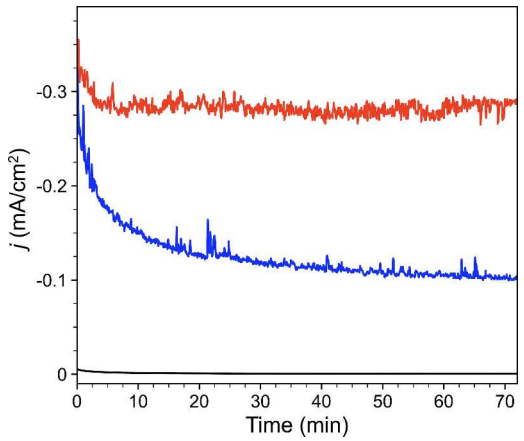

Figure 5. CPE current density traces for formate oxidation with **1** (0.35 mM, E_{app} = −0.80 V vs $Fc^{+/0}$, blue) or **2** (0.35 mM, E_{app} = −0.68 V vs $Fc^{+/0}$, red) with 50 equiv $[^nBu_4N][HCO_2]\cdot HCO_2H$ in acetonitrile. Control experiment in the absence of cobalt at E_{app} = −0.65 V vs $Fc^{+/0}$ (black).

headspace by gas chromatography confirmed CO_2 production with high faradaic efficiency (Table 3). Additionally, no CO

Table 3. Summary of Electrocatalytic Formate Oxidation Data

catalyst	k_{obs} (h^{-1})[a]	j (mA/cm^2)[b]	FE_{CO2} (%)[b]	TON at 95 min[c]	η_{CO2} (V)[d]
1	<4	−0.24 ± 0.03	99 ± 3	3.9 ± 0.9	0.45
2	135 ± 8	−0.09 ± 0.03	96 ± 3	10.7 ± 2.3	0.57
none	n/a	<0.001	n/a	n/a	n/a

[a]Average value from four CA trials. [b]Average value from three CPE trials for 95 min. [c]Calculated from the ratio of moles of CO_2 produced after 95 min and total moles of catalyst. [d]Calculated from the difference in $E_{1/2}(Co^{III}\text{-formate}/Co^{II})$ and $E^0(CO_2/HCOO^-)$.

production is observed. A turnover number (TON) of 10.7 ± 2.3 for **2** was achieved in only 95 min with no noticeable decay in the current density. CVs of the solution recorded post-electrolysis still show the $Co^{III/II}$ and $Co^{II/I}$ redox couples associated with **1** and **2**: ca. 75% of the catalyst remains intact based on the peak current of the $Co^{II/I}$ oxidation wave recorded before and after CPE (Figures S67−S70). The analogous CPE control experiments in the absence of cobalt catalyst show low current densities and negligible charge passed (Figure 5). Controlled-potential electrolysis with **3** under the same conditions did not result in productive electrocatalysis. Minimal current densities were achieved with this complex, and CVs recorded after electrolysis show no identifiable redox features. These results further demonstrate the decomposition of **3** at high concentrations of formate (*vide supra*).

The CA and CPE studies both indicate that **2** is the most active electrocatalyst in this series. We also probed the stability of **2** under the electrolysis conditions over longer time scales (Figure S71). The CPE current density for formate oxidation is initially stable and then gradually decreases over time. After 4.3 h, while maintaining the applied potential at the working electrode, the working electrode solution was spiked with more formate (50 equiv), resulting in an immediate increase in current density to ca. 70% of the starting value. The behavior indicates that the majority of the catalyst is still active at this point, and current decay is largely due to the decrease in formate concentration as the reaction proceeds. After 10 h, the electrolysis was stopped (ca. 27 turnovers), and CV analysis of the solution revealed ca. 40% of the catalyst remains intact. Thus, while clearly some decomposition of **2** occurs during operation, the catalyst structure maintains reasonable integrity and activity over several hours.

The overpotential for formate oxidation is estimated to be 0.45 and 0.57 V for **1** and **2**, respectively, based on the difference between the catalytic half-current potential (taken to be $E_{1/2}(Co^{III}\text{-formate}/Co^{II})$) and the standard thermodynamic potential for this reaction (E° = −1.40 V vs $Fc^{+/0}$).[24,55] The formate:formic acid buffer provides a sufficiently basic environment needed for deprotonation of the Co^{III}-hydride intermediate and electrocatalytic turnover, and thus formate is not only the substrate for formate oxidation but also serves as a base. The overall electrocatalytic reaction with **1** and **2** is therefore best given as the conversion of two equivalents of formate into one equivalent each of CO_2 and formic acid (Scheme 6). This is analogous to the Ni−P_2N_2, iridium, and

Scheme 6. Proposed Mechanism for Electrocatalytic Formate Oxidation with 1 and 2[a]

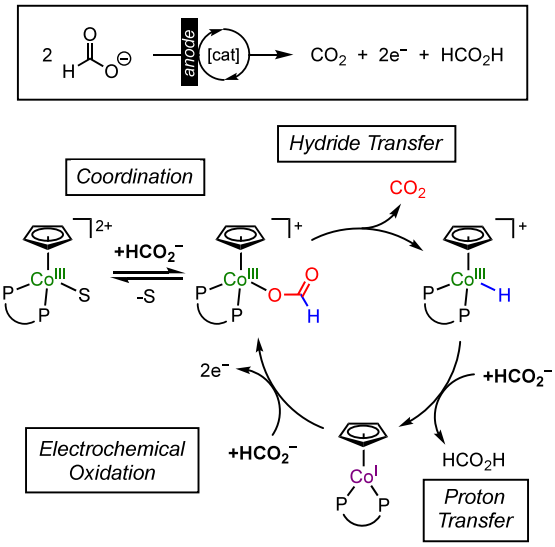

[a]S = acetonitrile.

iron electrocatalysts that also utilize formate as the base to achieve electrocatalytic turnover.[15,17,20] The overpotentials of **1** and **2** are comparable to the values reported for the Ni−P_2N_2 catalysts (η = 0.42−0.78 V).[56] The iridium catalyst reported by Kang and co-workers operates at a significantly larger overpotential (η = 1.25 V), though the catalytic rates of the nickel and iridium systems are faster than our cobalt catalysts.[37]

The observed reactivity of complexes **1** and **2** with formate depends on the reaction conditions. Initial formation of the Co^{III}-formate intermediate is followed by hydride transfer to generate the Co^{III}-hydride with the concomitant release of CO_2. The Co^{III}-hydride is weakly acidic and once formed, is deprotonated by the formate buffer to yield the Co^{I}

https://doi.org/10.1021/acscatal.4c03189
ACS Catal. 2025, 15, 1771−1781

intermediate. In the absence of applied potential, Co^{I} undergoes rapid comproportionation with the remaining Co^{III}−X (X = MeCN or formate) at low formate concentrations (Scheme 4), while at higher formate concentrations, the rate of hydride transfer is greatly increased and the complex remains in the Co^{I} state (Scheme 3). Under electrochemical conditions at an appropriate applied potential, electrocatalytic turnover is accessible via oxidation of Co^{I} at the electrode, regenerating the Co^{III}-formate and closing the cycle (Scheme 6). In this proposal, hydride transfer is reasonably assigned as the rate-limiting step.

The catalytic activity of **1** and **2** suggest the unique role of the pendent amines for promoting turnover. This conclusion is supported by the behavior of **3** and the related dcpa complex, which partially decomposes in the presence of excess formate or requires high temperatures for stoichiometric formate oxidation, respectively.[23] While the formate buffer may provide hydrogen bond donors to assist formate oxidation via intermolecular interactions,[57−59] the pendent amine arms in **1** and **2** may facilitate intramolecular hydrogen bonding stabilization.[60−64] Such transition state stabilization was proposed for CO_2 reduction to formate with **1**.[28] Given that the P_2N_2 has two pendent amine arms, a "pinched" hydrogen bonding conformation that restricts ligand movement may be accessible, which is calculated to be near ergoneutral with the nonpinched structure (Schemes S1 and S2).[65,66] Further studies to explore the conformational dynamics and pathways for hydride transfer with these complexes will be the subject of future work. Complex **3** is unable to provide intramolecular stabilization, allowing decomposition pathways—likely related to dppp ligand loss—to become kinetically competitive with formate oxidation. The nitrogen center in the dcpa complex[23] is nearly trigonal planar and has significantly reduced nucleophilicity compared to the P_2N_2 or PNP amines. Thus, despite the similar thermodynamic hydricities of these [CpCo] complexes (Table 2), the kinetic accessibility of formate oxidation significantly depends on the outer coordination sphere of the complex.

Both **1** and **2** are highly selective for CO_2 production and operate at modest overpotentials at 25 °C. These data unambiguously establish **1** and **2** as competent electrocatalysts for formate oxidation. This series marks the fifth example of a molecular electrocatalyst for this reaction and only the third catalyst family based on a first-row transition metal. Given the previously established CO_2 reduction activity of **1**,[28] this complex represents a rare example of a bidirectional electrocatalyst for the interconversion of CO_2 and formate. Finally, we highlight that **1** and **2** are the first homogeneous cobalt-based electrocatalysts for formate oxidation. Cobalt catalysts for the chemical dehydrogenation of formic acid are also exceedingly rare: only two examples have been reported.[67,68] Both chemical systems require elevated temperatures for catalytic turnover, which, similar to **1** and **2**, is proposed to involve rate-limiting hydride transfer for cleavage of the formate C−H bond and loss of CO_2.

CONCLUSION

Homogeneous electrocatalysts for formate oxidation are extremely limited, and only two previous reports have disclosed this activity at first-row transition metal systems. Herein, we have described a family of piano-stool cobalt complexes based on bidentate phosphine ligands that promote electrocatalytic formate oxidation. We have isolated three examples in this family in which the structure of the phosphine backbone was varied, and in each case the $[Co^{III}\text{-MeCN}]^{2+}$, $[Co^{I}]^{0}$, and $[Co^{III}\text{-hydride}]^{+}$ complexes were prepared. Detailed characterization of these complexes was performed to obtain key thermodynamic metrics. The thermodynamic hydricity of each Co^{III}-hydride indicated that hydride transfer from the formate anion to the Co^{III} center should be highly favorable in acetonitrile, which was confirmed through chemical reactivity studies. In addition, the acidity of the Co^{III}-hydride complexes is such that formate can also serve as a base to facilitate deprotonation, eliminating the need for a stronger exogeneous base. While the dppp complex **3** exhibited limited stability in the presence of formate, the P_2N_2 and PNP complexes **1** and **2** are active electrocatalysts, selectively affording CO_2 with excellent faradaic efficiency and marking the first cobalt-based examples of homogeneous electrocatalysts for formate oxidation. Complex **2** delivered the highest activity for formate oxidation, with the observed rate constant determined by CA being 135 h^{-1}. The pendent amine groups are critical for facilitating hydride transfer for formate oxidation, underscoring the important role of the catalyst outer coordination sphere. This work further revealed the unexpected result that a single pendent amine in the PNP ligand is more beneficial than the P_2N_2 ligand for formate oxidation, which will have important implications for the design of new catalysts for this and other electrocatalytic transformations.

METHODS AND MATERIALS

General Considerations. All operations were performed under inert atmosphere in an inert atmosphere glovebox or using standard Schlenk techniques, unless otherwise specified. All NMR spectra were collected at 25 °C unless otherwise indicated. ^{1}H, $^{13}C\{^{1}H\}$, and $^{31}P\{^{1}H\}$ NMR spectra were recorded on a Varian VNMRS 500 MHz spectrometer. Chemical shifts are reported in parts per million (δ). The chemical shifts of ^{1}H and ^{13}C nuclei were referenced using the residual solvent peaks (^{1}H NMR) or the characteristic resonances of the solvent nuclei as internal standards ($^{13}C\{^{1}H\}$ NMR). Electronic absorption spectra were recorded on an Agilent Cary 60 UV−vis spectrophotometer. Mass spectra was collected via an electrospray ionization source (ESI) with a Xevo G2-XS QTOF mass spectrometer in positive ion mode. Gas chromatography to quantify CO_2 production was performed using a Shimadzu GC-2014 gas chromatograph equipped with a methanizer fed into a flame ionization detector, a Restek Micropacked Shin Carbon column, and nitrogen carrier gas. Full details of X-ray data collection and refinement, electrochemical analysis, and computational studies are provided in the Supporting Information.

Materials. Acetonitrile and toluene were dried using a Pure Process Technology Solvent Purification System and then dried further over 3 Å molecular sieves. Diethyl ether was dried over 3 Å molecular sieves. Acetonitrile-d3 (99.8% D, Cambridge Isotope Laboratories) was dried over 3 Å molecular sieves. All solvents were degassed by three freeze−pump−thaw cycles and stored under an inert atmosphere. 1,3-Bis(diphenylphosphino)propane and $CpCo(CO)_2$ were purchased from Strem and used as received. Ferrocene and tetra-n-butylammonium hexafluorophosphate were purchased from Millipore Sigma and recrystallized from hexanes or ethanol, respectively. $CpCo(CO)I_2$,[69] $[^{n}Bu_4N][HCO_2]\cdot HCO_2H$,[14] and

https://doi.org/10.1021/acscatal.4c03189
ACS Catal. 2025, 15, 1771−1781

phosphine ligands ($P^{Ph}{}_2N^{Bn}{}_2$ and $P^{Ph2}N^{Bn}P^{Ph2}$)[38,39] were synthesized following literature procedures. All synthetic procedures and characterization details utilized in this work are provided in the Supporting Information.

■ ASSOCIATED CONTENT

Supporting Information

The Supporting Information is available free of charge at https://pubs.acs.org/doi/10.1021/acscatal.4c03189.

Complete experimental details and characterization data for prepared compounds, crystallographic details, additional electrochemical and spectroscopic data, computational details (PDF)

Cartesian coordinates for DFT-calculated structures (ZIP)

Accession Codes

CDCC 2227113−2227114, 2231484−2231487, and 2286870−2286872 contains the supplemental crystallographic data for this paper. These data can be obtained free of charge via www.ccdc.cam.ac.uk/data_request/cif, or by emailing data_request@ccdc.cam.ac.uk, or by contacting The Cambridge Crystallographic Data Centre, 12 Union Road, Cambridge CB2 1EZ, UK; fax: + 44 1223 336033.

■ AUTHOR INFORMATION

Corresponding Author

Kate M. Waldie − *Department of Chemistry and Chemical Biology, Rutgers, The State University of New Jersey, Piscataway, New Jersey 08854, United States;* orcid.org/0000-0001-6444-6122; Email: kate.waldie@rutgers.edu

Authors

Sriram Katipamula − *Department of Chemistry and Chemical Biology, Rutgers, The State University of New Jersey, Piscataway, New Jersey 08854, United States*

Andrew W. Cook − *Department of Chemistry and Chemical Biology, Rutgers, The State University of New Jersey, Piscataway, New Jersey 08854, United States;* orcid.org/0000-0002-8850-8946

Isabella Niedzwiecki − *Department of Chemistry and Chemical Biology, Rutgers, The State University of New Jersey, Piscataway, New Jersey 08854, United States*

Chathumini Nadeesha − *Department of Chemistry and Chemical Biology, Rutgers, The State University of New Jersey, Piscataway, New Jersey 08854, United States*

Ashish Parihar − *Department of Chemistry and Chemical Biology, Rutgers, The State University of New Jersey, Piscataway, New Jersey 08854, United States*

Thomas J. Emge − *Department of Chemistry and Chemical Biology, Rutgers, The State University of New Jersey, Piscataway, New Jersey 08854, United States;* orcid.org/0000-0002-5307-7250

Complete contact information is available at: https://pubs.acs.org/10.1021/acscatal.4c03189

Author Contributions

Conceptualization, S.K., A.W.C., and K.M.W.; methodology, S.K., A.W.C., A.P., and K.M.W.; investigation, S.K., A.W.C., I.N., C.N., A.P., and T.J.E.; writing−original draft, S.K. and K.M.W.; writing−review and editing, S.K., C.N., and K.M.W.; supervision, K.M.W.

Notes

The authors declare no competing financial interest.

A previous version of this manuscript was previously deposited as a preprint in ChemRxiv.[70]

■ ACKNOWLEDGMENTS

This work was supported by Rutgers, The State University of New Jersey. The Rigaku SYNERGY-S X-ray diffractometer was partially funded by an NSF MRI Award (CHE-2117792) to the Rutgers University Department of Chemistry and Chemical Biology. We thank Daniel Rothschild for assistance with mass spectrometry analysis. We also thank Prof. Jillian Dempsey for helpful discussions.

■ REFERENCES

(1) Lubitz, W.; Tumas, W. Hydrogen: An Overview. *Chem. Rev.* **2007**, *107* (10), 3900−3903.

(2) Oliveira, A. M.; Beswick, R. R.; Yan, Y. A green hydrogen economy for a renewable energy society. *Curr. Opin. Chem. Eng.* **2021**, *33*, No. 100701.

(3) Abe, J. O.; Popoola, A. P. I.; Ajenifuja, E.; Popoola, O. M. Hydrogen energy, economy and storage: Review and recommendation. *Int. J. Hydrogen Energy* **2019**, *44* (29), 15072−15086.

(4) *The Future of Hydrogen*; International Energy Agency, 2019.

(5) Preuster, P.; Papp, C.; Wasserscheid, P. Liquid Organic Hydrogen Carriers (LOHCs): Toward a Hydrogen-free Hydrogen Economy. *Acc. Chem. Res.* **2017**, *50* (1), 74−85.

(6) Eppinger, J.; Huang, K.-W. Formic Acid as a Hydrogen Energy Carrier. *ACS Energy Lett.* **2017**, *2* (1), 188−195.

(7) Li, Z.; Xu, Q. Metal-Nanoparticle-Catalyzed Hydrogen Generation from Formic Acid. *Acc. Chem. Res.* **2017**, *50* (6), 1449−1458.

(8) An, L.; Chen, R. Direct formate fuel cells: A review. *J. Power Sources* **2016**, *320*, 127−139.

(9) Yu, X.; Manthiram, A. Catalyst-selective, scalable membraneless alkaline direct formate fuel cells. *Appl. Catal., B* **2015**, *165*, 63−67.

(10) Xiong, Y.; Dong, J.; Huang, Z.-Q.; Xin, P.; Chen, W.; Wang, Y.; Li, Z.; Jin, Z.; Xing, W.; Zhuang, Z.; Ye, J.; Wei, X.; Cao, R.; Gu, L.; Sun, S.; Zhuang, L.; Chen, X.; Yang, H.; Chen, C.; Peng, Q.; Chang, C.-R.; Wang, D.; Li, Y. Single-atom Rh/N-doped carbon electrocatalyst for formic acid oxidation. *Nat. Nanotechnol.* **2020**, *15* (5), 390−397.

(11) Zhao, Y.; Zhang, K.; Li, Y.; Li, C.; Zhao, R.; Ji, Y.; Meng, Y.; Hu, T.; Wang, H.; Yang, Z.; Yan, Y.-M. Enhanced Electrocatalytic Oxidation of Formate via Introducing Surface Reactive Oxygen Species to a CeO_2 Substrate. *ACS Appl. Mater. Interfaces* **2021**, *13* (43), 51643−51651.

(12) Sun, H.-Y.; Ding, Y.; Yue, Y.-Q.; Zue, Q.; Li, F.-M.; Jiang, J.-X.; Chen, P.; Chen, Y. Bifunctional Palladium Hydride Nanodendrite Electrocatalysts for Hydrogen Evolution Integrated with Formate Oxidation. *ACS Appl. Mater. Interfaces* **2021**, *13* (11), 13149−13157.

(13) Guo, L.; Jin, T.; Tang, Q.; Wang, J.; Pan, B.; Wang, Q.; Li, Z.; Wang, C.; Liu, J.; Chen, F. Reconstruction of an AgPd nanoalloy with oxidation for formate oxidation electrocatalysis. *J. Mater. Chem. A* **2022**, *10* (26), 13998−14010.

(14) Galan, B. R.; Schöffel, J.; Linehan, J. C.; Seu, C.; Appel, A. M.; Roberts, J. A. S.; Helm, M. L.; Kilgore, U. J.; Yang, J. Y.; DuBois, D. L.; Kubiak, C. P. Electrocatalytic Oxidation of Formate by $[Ni(P^R{}_2N^{R'}{}_2)_2(CH_3CN)]^{2+}$ Complexes. *J. Am. Chem. Soc.* **2011**, *133* (32), 12767−12779.

(15) Seu, C. S.; Appel, A. M.; Doud, M. D.; DuBois, D. L.; Kubiak, C. P. Formate oxidation via β-deprotonation in $[Ni(P^R{}_2N^{R'}{}_2)_2(CH_3CN)]^{2+}$ complexes. *Energy Environ. Sci.* **2012**, *5* (4), 6480−6490.

(16) Galan, B. R.; Reback, M. L.; Jain, A.; Appel, A. M.; Shaw, W. J. Electrocatalytic Oxidation of Formate with Nickel Diphosphine

Dipeptide Complexes: Effect of Ligands Modified with Amino Acids. *Eur. J. Inorg. Chem.* **2013**, *2013* (30), 5366−5371.
(17) Bi, J.; Hou, P.; Kang, P. Single Iridium Pincer Complex for Roundtrip Electrochemical Conversion between Carbon Dioxide and Formate. *ChemCatChem.* **2019**, *11* (8), 2069−2072.
(18) Cunningham, D. W.; Barlow, J. M.; Velazquez, R. S.; Yang, J. Y. Reversible and Selective CO_2 to HCO_2^- Electrocatalysis near the Thermodynamic Potential. *Angew. Chem., Int. Ed.* **2020**, *59* (11), 4443−4447.
(19) Xue, L.; Ahlquist, M. S. G. A DFT Study: Why Do $[Ni(P^R_2N^{R'}_2)_2]^{2+}$ Complexes Facilitate the Electrocatalytic Oxidation of Formate? *Inorg. Chem.* **2014**, *53* (7), 3281−3289.
(20) Li, Y.; Chen, J.-Y.; Zhang, X.; Peng, Z.; Miao, Q.; Chen, W.; Xie, F.; Liao, R.-Z.; Ye, S.; Tung, C.-H.; Wang, W. Electrocatalytic Interconversions of CO_2 and Formate on a Versatile Iron-Thiolate Platform. *J. Am. Chem. Soc.* **2023**, *145* (49), 26915−26924.
(21) Wiedner, E. S.; Chambers, M. B.; Pitman, C. L.; Bullock, R. M.; Miller, A. J. M.; Appel, A. M. Thermodynamic Hydricity of Transition Metal Hydrides. *Chem. Rev.* **2016**, *116* (15), 8655−8692.
(22) DuBois, D. L.; Berning, D. E. Hydricity of transition-metal hydrides and its role in CO_2 reduction. *Appl. Organomet. Chem.* **2000**, *14* (12), 860−862.
(23) Cook, A. W.; Emge, T. J.; Waldie, K. M. Insights into Formate Oxidation by a Series of Cobalt Piano-Stool Complexes Supported by Bis(phosphino)amine Ligands. *Inorg. Chem.* **2021**, *60* (10), 7372−7380.
(24) Waldie, K. M.; Ostericher, A. L.; Reineke, M. H.; Sasayama, A. F.; Kubiak, C. P. Hydricity of Transition-Metal Hydrides: Thermodynamic Considerations for CO_2 Reduction. *ACS Catal.* **2018**, *8* (2), 1313−1324.
(25) Fang, M.; Wiedner, E. S.; Dougherty, W. G.; Kassel, W. S.; Liu, T.; DuBois, D. L.; Bullock, R. M. Cobalt Complexes Containing Pendant Amines in the Second Coordination Sphere as Electrocatalysts for H_2 Production. *Organometallics* **2014**, *33* (20), 5820−5833.
(26) Koelle, U.; Paul, S. Electrochemical reduction of protonated cyclopentadienylcobalt phosphine complexes. *Inorg. Chem.* **1986**, *25* (16), 2689−2694.
(27) van der Meer, M.; Glais, E.; Siewert, I.; Sarkar, B. Electrocatalytic Dihydrogen Production with a Robust Mesoionic Pyridylcarbene Cobalt Catalyst. *Angew. Chem., Int. Ed.* **2015**, *54* (46), 13792−13795.
(28) Roy, S.; Sharma, B.; Pécaut, J.; Simon, P.; Fontecave, M.; Tran, P. D.; Derat, E.; Artero, V. Molecular Cobalt Complexes with Pendant Amines for Selective Electrocatalytic Reduction of Carbon Dioxide to Formic Acid. *J. Am. Chem. Soc.* **2017**, *139* (10), 3685−3696.
(29) Curtis, C. J.; Miedaner, A.; Ciancanelli, R.; Ellis, W. W.; Noll, B. C.; Rakowski DuBois, M.; DuBois, D. L. $[Ni(Et_2PCH_2NMeCH_2PEt_2)_2]^{2+}$ as a Functional Model for Hydrogenases. *Inorg. Chem.* **2003**, *42* (1), 216−227.
(30) Helm, M. L.; Stewart, M. P.; Bullock, R. M.; DuBois, M. R.; DuBois, D. L. A Synthetic Nickel Electrocatalyst with a Turnover Frequency Above 100,000 s^{-1} for H_2 Production. *Science* **2011**, *333* (6044), 863−866.
(31) Liu, T.; DuBois, D. L.; Bullock, R. M. An iron complex with pendent amines as a molecular electrocatalyst for oxidation of hydrogen. *Nat. Chem.* **2013**, *5* (3), 228−233.
(32) Yang, J. Y.; Bullock, R. M.; Dougherty, W. G.; Kassel, W. S.; Twamley, B.; DuBois, D. L.; Rakowski DuBois, M. Reduction of oxygen catalyzed by nickel diphosphine complexes with positioned pendant amines. *Dalton Trans.* **2010**, *39* (12), 3001−3010.
(33) Weiss, C. J.; Egbert, J. D.; Chen, S.; Helm, M. L.; Bullock, R. M.; Mock, M. T. Protonation Studies of a Tungsten Dinitrogen Complex Supported by a Diphosphine Ligand Containing a Pendant Amine. *Organometallics* **2014**, *33* (9), 2189−2200.
(34) Weiss, C. J.; Wiedner, E. S.; Roberts, J. A. S.; Appel, A. M. Nickel phosphine catalysts with pendant amines for electrocatalytic oxidation of alcohols. *Chem. Commun.* **2015**, *51* (28), 6172−6174.
(35) Bhattacharya, P.; Heiden, Z. M.; Wiedner, E. S.; Raugei, S.; Piro, N. A.; Kassel, W. S.; Bullock, R. M.; Mock, M. T. Ammonia Oxidation by Abstraction of Three Hydrogen Atoms from a Mo−NH_3 Complex. *J. Am. Chem. Soc.* **2017**, *139* (8), 2916−2919.
(36) Wiedner, E. S.; Appel, A. M.; Raugei, S.; Shaw, W. J.; Bullock, R. M. Molecular Catalysts with Diphosphine Ligands Containing Pendant Amines. *Chem. Rev.* **2022**, *122* (14), 12427−12474.
(37) Waldie, K. M.; Katipamula, S. Recent Progress in the Development of Molecular Electrocatalysts for Formate Oxidation. *Catalysis Research* **2021**, *02* (01), No. 2201006.
(38) Weiss, C. J.; Groves, A. N.; Mock, M. T.; Dougherty, W. G.; Kassel, W. S.; Helm, M. L.; DuBois, D. L.; Bullock, R. M. Synthesis and reactivity of molybdenum and tungsten bis(dinitrogen) complexes supported by diphosphine chelates containing pendant amines. *Dalton Trans.* **2012**, *41* (15), 4517−4529.
(39) Fraze, K.; Wilson, A. D.; Appel, A. M.; Rakowski DuBois, M.; DuBois, D. L. Thermodynamic Properties of the Ni−H Bond in Complexes of the Type $[HNi(P_2^RN_2^{R'})_2](BF_4)$ and Evaluation of Factors That Control Catalytic Activity for Hydrogen Oxidation/Production. *Organometallics* **2007**, *26* (16), 3918−3924.
(40) Waldie, K. M.; Kim, S.-K.; Ingram, A. J.; Waymouth, R. M. Cyclopentadienyl Cobalt Complexes as Precatalysts for Electrocatalytic Hydrogen Evolution. *Eur. J. Inorg. Chem.* **2017**, *2017* (20), 2755−2761.
(41) Kurtz, D. A.; Dhar, D.; Elgrishi, N.; Kandemir, B.; McWilliams, S. F.; Howland, W. C.; Chen, C.-H.; Dempsey, J. L. Redox-Induced Structural Reorganization Dictates Kinetics of Cobalt(III) Hydride Formation via Proton-Coupled Electron Transfer. *J. Am. Chem. Soc.* **2021**, *143* (9), 3393−3406.
(42) Elgrishi, N.; Kurtz, D. A.; Dempsey, J. L. Reaction Parameters Influencing Cobalt Hydride Formation Kinetics: Implications for Benchmarking H_2-Evolution Catalysts. *J. Am. Chem. Soc.* **2017**, *139* (1), 239−244.
(43) Berning, D. E.; Noll, B. C.; DuBois, D. L. Relative Hydride, Proton, and Hydrogen Atom Transfer Abilities of $[HM(diphosphine)_2]PF_6$ Complexes (M = Pt, Ni). *J. Am. Chem. Soc.* **1999**, *121* (49), 11432−11447.
(44) Brereton, K. R.; Smith, N. E.; Hazari, N.; Miller, A. J. M. Thermodynamic and kinetic hydricity of transition metal hydrides. *Chem. Soc. Rev.* **2020**, *49* (22), 7929−7948.
(45) Tshepelevitsh, S.; Kütt, A.; Lõkov, M.; Kaljurand, I.; Saame, J.; Heering, A.; Plieger, P. G.; Vianello, R.; Leito, I. On the Basicity of Organic Bases in Different Media. *Eur. J. Org. Chem.* **2019**, *2019* (40), 6735−6748.
(46) Raebiger, J. W.; Miedaner, A.; Curtis, C. J.; Miller, S. M.; Anderson, O. P.; DuBois, D. L. Using Ligand Bite Angles To Control the Hydricity of Palladium Diphosphine Complexes. *J. Am. Chem. Soc.* **2004**, *126* (17), 5502−5514.
(47) Curtis, C. J.; Miedaner, A.; Raebiger, J. W.; DuBois, D. L. Periodic Trends in Metal Hydride Donor Thermodynamics: Measurement and Comparison of the Hydride Donor Abilities of the Series $HM(PNP)^{2+}$ (M = Ni, Pd, Pt; PNP = $Et_2PCH_2N(Me)CH_2PEt_2$). *Organometallics* **2004**, *23* (3), 511−516.
(48) Stirling, M. J.; Sweeney, G.; MacRory, K.; Blacker, A. J.; Page, M. I. The kinetics and mechanism of the organo-iridium-catalysed enantioselective reduction of imines. *Org. Biomol. Chem.* **2016**, *14* (14), 3614−3622.
(49) Katipamula, S.; Nadeesha, C.; Emge, T. J.; Waldie, K. M. Oxidation-Induced Ligand Swap: Oxygen Insertion into a Cobalt-Phosphine Complex. *Organometallics* **2024**, *43* (18), 2036−2043.
(50) Zhang, Y.; MacIntosh, A. D.; Wong, J. L.; Bielinski, E. A.; Williard, P. G.; Mercado, B. Q.; Hazari, N.; Bernskoetter, W. H. Iron catalyzed CO_2 hydrogenation to formate enhanced by Lewis acid co-catalysts. *Chem. Sci.* **2015**, *6* (7), 4291−4299.
(51) The ^1H NMR chemical shift of the formyl C−H protons in $[^nBu_4N][HCO_2]\cdot HCO_2H$ varied from 8.52 to 8.69 ppm, indicating different formate:formic acid ratios were obtained in different batches.
(52) Bard, A. J.; Faulkner, L. R. *Electrochemical Methods: Fundamentals and Applications*, 2nd ed.; John Wiley & Sons: 2001.

https://doi.org/10.1021/acscatal.4c03189
ACS Catal. 2025, 15, 1771−1781

(53) Kurtz, D. A.; Dempsey, J. L. Proton-coupled electron transfer kinetics for the photoinduced generation of a cobalt(III)-hydride complex. *Inorg. Chem.* **2019**, *58* (24), 16510−16517.
(54) Delahay, P.; Stiehl, G. L. Theory of Catalytic Polarographic Currents. *J. Am. Chem. Soc.* **1952**, *74* (14), 3500−3505.
(55) Appel, A. M.; Helm, M. L. Determining the overpotential for a molecular electrocatalyst. *ACS Catal.* **2014**, *4* (2), 630−633.
(56) Waldie, K. M.; Brunner, F. M.; Kubiak, C. P. Transition Metal Hydride Catalysts for Sustainable Interconversion of CO_2 and Formate: Thermodynamic and Mechanistic Considerations. *ACS Sustainable Chem. Eng.* **2018**, *6* (5), 6841−6848.
(57) Pavlovic, L.; Hopmann, K. H. Understanding the Influence of Lewis Acids on CO_2 Hydrogenation: The Critical Effect Is on Formate Rotation. *Organometallics* **2023**, *42* (20), 3025−3035.
(58) Osipova, E. S.; Sedlova, D. V.; Gutsul, E. I.; Nelyubina, Y. V.; Dorovatovskii, P. V.; Epstein, L. M.; Filippov, O. A.; Shubina, E. S.; Belkova, N. V. Reactivity of Heterobimetallic Ion Pairs in Formic Acid Dehydrogenation. *Organometallics* **2023**, *42* (18), 2651−2660.
(59) Bielinski, E. A.; Lagaditis, P. O.; Zhang, Y.; Mercado, B. Q.; Würtele, C.; Bernskoetter, W. H.; Hazari, N.; Schneider, S. Lewis Acid-Assisted Formic Acid Dehydrogenation Using a Pincer-Supported Iron Catalyst. *J. Am. Chem. Soc.* **2014**, *136* (29), 10234−10237.
(60) Reek, J. N. H.; de Bruin, B.; Pullen, S.; Mooibroek, T. J.; Kluwer, A. M.; Caumes, X. Transition Metal Catalysis Controlled by Hydrogen Bonding in the Second Coordination Sphere. *Chem. Rev.* **2022**, *122* (14), 12308−12369.
(61) Taylor, R.; Kennard, O.; Versichel, W. Geometry of the N-H···O═C hydrogen bond. 2. Three-center ("bifurcated") and four-center ("trifurcated") bonds. *J. Am. Chem. Soc.* **1984**, *106* (1), 244−248.
(62) Aakeröy, C. B.; Seddon, K. R. The hydrogen bond and crystal engineering. *Chem. Soc. Rev.* **1993**, *22*, 397−407.
(63) Rozas, I.; Alkorta, I.; Elguero, J. Bifurcated Hydrogen Bonds: Three-Centered Interactions. *J. Phys. Chem. A* **1998**, *102* (48), 9925−9932.
(64) Karas, L. J.; Wu, C.-H.; Das, R.; Wu, J. I.-C. Hydrogen bond design principles. *WIREs Comput. Mol. Sci.* **2020**, *10*, No. e1477.
(65) O'Hagan, M.; Ho, M.-H.; Yang, J. Y.; Appel, A. M.; Rakowski DuBois, M.; Raugei, S.; Shaw, W. J.; DuBois, D. L.; Bullock, R. M. Proton Delivery and Removal in $[Ni(P^R_2N^{R'}_2)_2]^{2+}$ Hydrogen Production and Oxidation Catalysts. *J. Am. Chem. Soc.* **2012**, *134* (47), 19409−19424.
(66) Bullock, R. M.; Helm, M. L. Molecular Electrocatalysts for Oxidation of Hydrogen Using Earth-Abundant Metals: Shoving Protons Around with Proton Relays. *Acc. Chem. Res.* **2015**, *48* (7), 2017−2026.
(67) Zhou, W.; Wei, Z.; Spannenberg, A.; Jiao, H.; Junge, K.; Junge, H.; Beller, M. Cobalt-Catalyzed Aqueous Dehydrogenation of Formic Acid. *Chem.—Eur. J.* **2019**, *25* (36), 8459−8464.
(68) Lentz, N.; Aloisi, A.; Thuéry, P.; Nicolas, E.; Cantat, T. Additive-Free Formic Acid Dehydrogenation Catalyzed by a Cobalt Complex. *Organometallics* **2021**, *40* (5), 565−569.
(69) King, R. B. Organometallic Chemistry of the Transition Metals. XI. Some New Cyclopentadienyl Derivatives of Cobalt and Rhodium. *Inorg. Chem.* **1966**, *5* (1), 82−87.
(70) Katipamula, S.; Cook, A. W.; Niedzwiecki, I.; Emge, T. J.; Waldie, K. M., Electrocatalytic Formate Oxidation by Cobalt-Phosphine Complexes. *ChemRxiv* 2023, DOI: 10.26434/chemrxiv-2023-tfn6t. Accessed 2024−08−22.

https://doi.org/10.1021/acscatal.4c03189
ACS Catal. 2025, 15, 1771−1781